INTERNATIONAL JOURNAL FOR NUMERICAL METHODS IN FLUIDS, VOL. 3, 605–622 (1983)

A STREAM FUNCTION FINITE ELEMENT SOLUTION FOR TWO-DIMENSIONAL NATURAL CONVECTION WITH ACCURATE REPRESENTATION OF NUSSELT NUMBER VARIATIONS NEAR A CORNER

P. L. BETTS AND V. HAROUTUNIAN

Department of Mechanical Engineering, University of Manchester Institute of Science and Technology, P.O. Box 88, Manchester M60 1QD, England

SUMMARY

A finite element stream function formulation is presented for the solution to the two-dimensional double-glazing problem. Laminar flow with constant properties is considered and the Boussinesq approximation used. A restricted variational principle is used, in conjunction with a triangular finite element of C^1 continuity, to discretize the two coupled governing partial differential equations (4th order in stream function and second order in temperature). The resulting non-linear system of equations is solved in a segregated (decoupled) manner by the Newton–Raphson linearizing technique.

Results are produced for the standard test case of an upright square cavity. These are for Rayleigh numbers in the range 10^3–10^5, with a Prandtl number of 0·71. Comparisons are made with benchmark results presented at the 1981 International Comparison study in Venice. In the discussion of results, emphasis is placed on the variation of local Nusselt number along the isothermal walls, particularly near the corner. This reveals a noticeable source of error in the evaluation of the maximum Nusselt number by lower order discretization methods.

KEY WORDS Natural Convection Stream Function Finite Element Formulation C^1 Continuity Truncated Quintic Restricted Variational Principle.

1. INTRODUCTION

The occurrence of natural convection in many practical flow situations, its influence on the transport processes, and the need for a quantitative account of its behaviour requires little introduction.

In most cases of environmental and engineering interest natural convection gives rise to turbulent flows. However, as a logical step in the direction towards modelling these flows, one requires to be able to solve the less complex laminar natural convection flows. It is for this reason that laminar natural convection has attracted considerable recent interest. The most popular test case for the solution of these flows has been the two-dimensional 'double-glazing' problem. The attractive features of this test problem are that it has a simple geometry, it has no singularities and buoyancy is the only driving mechanism for the flow.

Numerical simulations of the double-glazing problem have been extremely varied in their choice of mathematical model, formulation strategy, discretization scheme and solution

---

This invited paper is an extended, and refereed version of one presented at the Fourth International Symposium on Finite Elements in Flow Problems held in Tokyo, Japan, 26–29 July 1982.

0271–2091/83/060605–18$01.80

Received 27 January 1983
Revised 20 June 1983

strategy. The mathematical model used by most authors today is the constant fluid property model with the Boussinesq approximation for density changes. This model, which is particularly convenient for comparison purposes, is presented in the next section. There are a number of basic ways in which it can be formulated. Three of these consist of formulating the hydrodynamic part of the problem in terms of the 'primitive variables' ($\mathbf{u}$, p), in terms of stream function and vorticity (ψ–ω) or in terms of stream function (ψ) only.

The primitive variables formulation strategy, although very successful and indeed popular with many authors, suffers from difficulties in the numerical solution to the discretized system of equations. The difficulties are associated with the incompressible version of the governing equations. In this version the pressure variable appears in an implicit fashion in the governing equations. As a direct result of this, certain discretizations of the above mentioned governing equations produce 'free pressure modes'. These 'free modes' are readily excited by machine round-off and contaminate pressure (and in some instances velocity) solutions. Other discretizations on the other hand do not produce spurious pressure solutions, but fail to strike an adequate balance between the number of vector momentum and continuity equations.

The interesting and methodical studies of Sani *et al*[1] and Jackson and Cliffe[2] demonstrate and discuss the above mentioned problems in the context of the Galerkin finite element method (GFEM). In these, the causes of the problems are pointed out and techniques are devised for their suppression or elimination by way of mixed interpolations, proper choices of elements, element distributions and boundary conditions.

The stream function–vorticity (ψ–ω) model does not suffer from the above limitations. It has, however, a unique restriction, this being due to the fact that vorticity boundary values are not known *a priori*. In the majority of such simulations,[3,4] approximate vorticity boundary values are arrived at, during the course of the solution, by extrapolating to the boundary using the latest available field variables. These extrapolation techniques are generally not consistent with the overall numerical scheme. That is, in such cases non-zero velocities at no-slip impermeable boundaries may result if the same extrapolation method were to be applied to the field variables for obtaining boundary velocities. A recent development in this area is the work of Stevens.[5] In his GFEM simulation of the double-glazing problem, he dispenses with the conventional extrapolation methods by providing gradient boundary conditions for vorticity which are consistent with the overall GFEM. This 'weak' imposition method of the vorticity boundary conditions, however, is unique to the GFEM and does not extend to other numerical methods.

The stream function (ψ) formulation strategy is free of the difficulties plaguing the ($\mathbf{u}$, p) and (ψ–ω) formulation strategies. Most fluid problems posed in this fashion have well defined boundary conditions and the discretized systems of equations associated with this formulation strategy do not tolerate 'free modes'. However, very few contributions have appeared in the literature which use this strategy, despite the above mentioned attractive features. The fourth order stream function partial differential equation resulting from this strategy seems to have deterred many authors from attempting a numerical solution. In the finite element context, Tuann and Olson[6,7] have solved the hydrodynamic equations using a restricted variational principle in conjunction with an 18 degree of freedom (DOF) triangular finite element of the C^1 continuity class. They have applied this method to both the isothermal flow in a driven cavity[6] and around a circular cylinder.[7]

In the present paper the method of Tuann and Olson is extended to include the energy equation to allow for the solution of natural convection. The way in which this is done is given in Section 3. The results of the present simulation are presented in Section 6. In

Section 7 comparisons are made between the present results and the benchmark results of de Vahl Davis.[8] The benchmark solution is a result of an international comparison exercise[9] which attracted worldwide interest.

2. MATHEMATICAL MODEL AND FORMULATION STRATEGY

Figure 1 indicates the problem in question; although the computed results presented in this paper are restricted to $\phi = 0{\cdot}0$ and $l = d$. The complete mathematical model for describing laminar natural convection in the box of Figure 1 can be arrived at from the statements of conservation of mass, momentum and energy in conjunction with constitutive equations which close the system by describing the state of the fluid. The mathematical model employed here is the simplified steady state version of the above statements with constant fluid properties and the Boussinesq approximation for density changes. The resulting dimensionless differential equations are as follows:

$$u\frac{\partial u}{\partial x}+v\frac{\partial u}{\partial y}=-\frac{\partial p}{\partial x}-Gr\theta\cos\phi+\nabla^2 u \tag{1a}$$

$$u\frac{\partial v}{\partial x}+v\frac{\partial v}{\partial y}=-\frac{\partial p}{\partial y}-Gr\theta\sin\phi+\nabla^2 v \tag{1b}$$

$$\frac{\partial u}{\partial x}+\frac{\partial v}{\partial y}=0 \tag{1c}$$

$$u\frac{\partial \theta}{\partial x}+v\frac{\partial \theta}{\partial y}=\frac{1}{Pr}\nabla^2\theta \tag{1d}$$

where the symbols have their conventional meanings, p is the pressure deviation from hydrostatic, $Gr = g\beta(T_H - T_C)d^3/\nu^2$ is the Grashoff number, $Pr = \nu/\alpha$ is the Prandtl number, β is the thermal expansion coefficient of the fluid, ν and α are the diffusion coefficients for momentum and heat. Note that $Ra = Gr.Pr$ is the Rayleigh number.

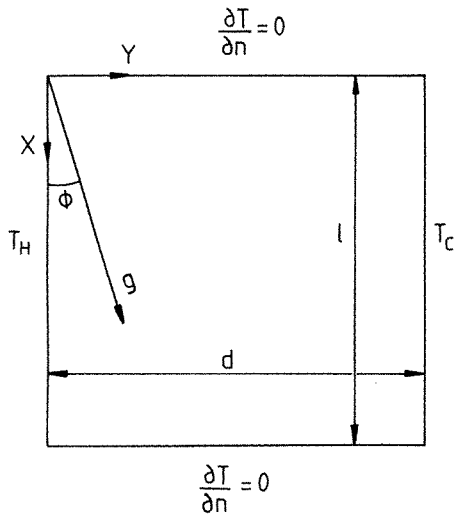

Figure 1. The square cavity

The non-dimensionalization scheme used in equations (1) is that used by Taborrok and Lin,[3] which gives non-dimensional velocities in Reynolds number form (Ud/ν where U denotes a dimensional velocity). Temperatures are referenced to the cold wall temperature, i.e. $\theta = (T - T_C)/(T_H - T_C)$. For comparison purposes, however, the results of this study are presented in a form consistent with the non-dimensionalization of Mallinson and de Vahl Davis[10] (i.e. $u = Ud/\alpha$).

The system of equations (1) is in primitive variable form (u, v, p, θ). It is possible to reformulate this in stream function–vorticity (ψ–ω, θ), or stream function (ψ, θ) form. Here the latter formulation strategy is adopted. By defining the stream function as $u = \psi_y$, $v = -\psi_x$, one arrives at

$$\nabla^4\psi - \psi_y(\nabla^2\psi)_x + \psi_x(\nabla^2\psi)_y - Gr(\theta_y \cos\phi - \theta_x \sin\phi) = 0 \tag{2a}$$

$$\theta_x\psi_y - \theta_y\psi_x - \frac{1}{Pr}\nabla^2\theta = 0 \tag{2b}$$

where subscripts denote partial derivatives. It is clearly seen here that a reduction in the number of variables of the governing system of equations (1) has been gained at the expense of admitting higher order derivatives in (2).

3. DISCRETIZATION SCHEME AND SOLUTION STRATEGY

There are no exact variational principles for the two equations of (2); this is due to their non-self adjoint convection terms. Consequently an *ad hoc* principle is used here, which is based on that developed by Tuann and Olson[6,7] for isothermal flow without buoyancy effects and is extended to the heat transfer situation.

Multiplying (2a) by a virtual displacement $\delta\psi$ and (2b) by $\delta\theta$, integrating each over the flow domain Ω, and applying the Gauss–Green theorem yields:

$$\iint_\Omega [\nabla^2\psi\nabla^2(\delta\psi) + (\psi_y\nabla^2\psi)(\delta\psi)_x - (\psi_x\nabla^2\psi)(\delta\psi)_y - GrS\,\delta\psi]\,d\Omega + \int_\Gamma [\nabla^2\psi_n - \nabla^2\psi(\mathbf{n}\times\nabla\psi)]\,\delta\psi\,d\Gamma - \int_\Gamma \nabla^2\psi\,\delta\psi_n\,d\Gamma = 0 \tag{3a}$$

$$\frac{1}{Pr}\int_\Gamma \left(\frac{\partial\theta}{\partial\mathbf{n}}\right)\delta\theta\,d\Gamma - \frac{1}{Pr}\iint_\Omega (\theta_x\,\delta\theta_x + \theta_y\,\delta\theta_y)\,d\Omega + \iint_\Omega [\theta_y\psi_x - \theta_x\psi_y]\,\delta\theta\,d\Omega = 0 \tag{3b}$$

where Γ is the whole boundary of the domain Ω, $\mathbf{n}$ is the outward pointing unit normal vector, δ is the variational operator and $S = \theta_y \cos\phi - \theta_x \sin\phi$. For the test case in question there is no contribution from the line integrals of (3). This is due to the rigid boundary conditions of zero streamline ($\psi = 0$ is arbitrarily defined on the connected walls), and no-slip impermeable walls in (3a) and to the rigid and natural boundary conditions of prescribed temperature on Γ_1 and insultation on Γ_2 in (3b) where $\Gamma = \Gamma_1 + \Gamma_2$. Therefore no variation is allowed in $\psi(\delta\psi = 0$, on $\Gamma)$, in $\psi_n(\delta\psi_n = 0$, on $\Gamma)$, nor in θ on $\Gamma_1(\delta\theta = 0$, on $\Gamma_1)$; moreover $\dfrac{\partial\theta}{\partial\mathbf{n}} = 0$ on Γ_2.

Extracting the variational operator δ from (3) yields the two restricted functionals to be minimized, namely:

$$I_1(\psi, \psi^0) = \iint_\Omega [\tfrac{1}{2}(\nabla^2\psi)^2 + (\psi_y^0\nabla^2\psi^0)\psi_x - (\psi_x^0\nabla^2\psi^0)\psi_y - GrS^*\psi]\,d\Omega \tag{4a}$$

$$I_2(\theta, \theta^0) = \frac{1}{2Pr}\iint_\Omega [(\theta_x)^2 + (\theta_y)^2]\,d\Omega + \iint_\Omega [\theta_x^0\psi_y^* - \theta_y^0\psi_x^*]\theta\,d\Omega \tag{4b}$$

Note that the superscript (zero) in (4) denotes that the variable remains fixed when the variation is taken and is regarded to be a variable again only after the variation (hence the reason for calling it the restricted variational principle). Moreover the superscript (asterisk) denotes coupling terms which are fixed in the appropriate variation.

This process then yields (2a) and (2b) as the Euler–Lagrange equations along with the rigid and natural boundary conditions previously specified. The 18 DOF truncated quintic triangular finite element of the C^1 continuity class was used to satisfy the C^1 continuity requirement of functional (4a). This finite element was developed in the context of plate bending analysis where the biharmonic operator (i.e. ∇^4) also appears in the system equations governing deflection. It is for this reason that the element is sometimes referred to as the high precision plate bending element. A brief introduction to this element and its nodal degrees of freedom is given in the next section.

The same element is also used to describe the approximation for θ in (4). Although convenient this is not strictly necessary, since the continuity requirement of (4b) is only C^0. This was however done, because the problem in question is essentially a heat transfer one and an accurate representation of the heat problem is obviously desirable. In this way the temperature and the heat flux vector become C^1 and C^0 continuous (respectively) in the solution domain and this is in contrast with most other simulations to the double glazing problem where C^0 and C^{-1} basis functions are used for the temperature and the heat flux vector.

Discretization of (4) is achieved by the following steps. Apply the functions of (4) to a typical element e. The integrations are now taken over the element area Ω^e and the derivatives in (4) are taken with respect to a local co-ordinate system (ξ, η) defined in element e. The polynomial representations for ψ and θ at the element level allow one to perform the analytical integrations over Ω^e. The matrix expressions for $I_1^e(\psi, \psi^0)$ and $I_2^e(\theta, \theta^0)$ thus obtained are expressed in terms of the local co-ordinates. Transform these expressions to the global (x, y) co-ordinate system and assemble in the global matrices representing the discretized form of (4). This process is repeated for all the elements in the solution domain for assembling the complete discretized form of (4). Performing the restricted variation of the discretized equivalents of the two functionals in (4), with respect to the stream function and temperature respectively, yields for arbitrary nodal variations of $\delta\boldsymbol{\psi}$ and $\delta\boldsymbol{\theta}$ equations of the form

$$\sum_{j=1}^{NS} K_{kj}\psi_j + \frac{1}{2}\sum_{i=1}^{NS}\sum_{j=1}^{NS} Q_{ijk}\psi_i\psi_j - GrG_k = 0, \qquad k = 1, 2, \ldots, NS \tag{5a}$$

$$\sum_{j=1}^{NT} M_{kj}\theta_j = 0, \qquad k = 1, 2, \ldots, NT \tag{5b}$$

$\boldsymbol{\psi}$ and $\boldsymbol{\theta}$ are the global vectors representing stream function and temperature 'nodal values' consistent with the Hermitian basis functions given by the C^1 class 18 DOF triangular finite element. That is, these vectors contain nodal values of the function, its two first derivatives and three second derivatives, a total of six DOF per vertex of the triangular finite element. **M**, **K**, **Q** and **G** are global operators representing diffusion, advection and body forces. *NS* is the size of the unknown stream function problem and similarly *NT* is the global number of free degrees of freedom associated with the heat transfer part of the problem.

A full account of the discretization procedure, beginning from (2) to (5), is given by Haroutunian,[11] where the element level equivalents of the above advection, diffusion and buoyancy operators are also defined. The procedure for the hydrodynamic terms only can also be seen from Tuann and Olsen.[6,7]

Equation (5b) is a non-symmetric system of linear equations, whereas (5a) is a set of $NS \times NS$ non-linear algebraic equations for the *NS* global unknowns ψ_i. Applying the Newton–Raphson linearizing technique to (5a) leads to the following two sets of non-symmetric linear equations.

$$\left[\sum_{i=1}^{NS} K_{ki} + \sum_{i=1}^{NS}\sum_{j=1}^{NS} Q_{ijk}\psi_j^n\right]\Delta\psi_i + F_k(\boldsymbol{\psi}^n) = 0, \qquad k = 1, 2, \ldots, NS \tag{6a}$$

$$\sum_{j=1}^{NT} M_{kj}\theta_j = 0, \qquad k = 1, 2, \ldots, NT \tag{6b}$$

where superscript n denotes the nth Newton–Raphson iteration, $\Delta\psi_i = \psi_i^{n+1} - \psi_i^n$ is the residual stream function vector, $F_k(\boldsymbol{\psi}^n)$ is the residual of the kth equation of (5a) at iteration level n, and the term in brackets in (6a) is the Jacobian matrix.

System (6) is solved in a segregated (decoupled) fashion until $\boldsymbol{\psi}$ and $\boldsymbol{\theta}$ converge to a solution, if at all. This solution strategy requires the starred terms in (4) to be treated as source terms, where at a given iteration level their value is prescribed from the previous iteration step. The criterion chosen for establishing convergence is a pre-assigned tolerance ε which is defined as the ratio of the Euclidean norms of $\Delta\boldsymbol{\psi}$ and $\boldsymbol{\psi}$ in percentage form, i.e. $\varepsilon = [\|\Delta\boldsymbol{\psi}\|/\|\boldsymbol{\psi}\|] \times 100$ per cent. The computer program developed for the numerical simulation allows for a variety of choices for damping during the course of the solution. Experience showed that a single Newton–Raphson iteration per equation step was appropriate for all flow situations, with the latest temperature value only damped for cases when the Rayleigh number was high. The degree of temperature update damping increased with increasing *Ra*. Further details on damping are given later.

4. THE 18-DOF TRIANGULAR FINITE ELEMENT

In this section only a brief description of the 18-DOF truncated quintic triangular finite element is given. The expressions relating the nodal values of the field variables to the polynomial coefficients, and the way in which these expressions are derived are given more fully in Reference 12.

The general field variable f (ψ or θ in the present problem) would require 21 polynomial terms, if it were to be represented locally in the element in terms of a complete quintic polynomial. Since the element can only allow for 18 degrees of freedom (i.e. six at each vertex) three additional constraints are thus needed. These additional conditions stipulate that the normal derivatives of the function f along each edge, f_n, be a cubic function of the edgewise co-ordinate s, where (s, n) is a co-ordinate system local to each side of the triangle.

For a full account of how these conditions are enforced by truncating the complete quintic polynomial of f see Reference 13.

Now the cubic polynomials f_n along each edge are uniquely defined by f_n and f_{ns} at each of the two terminal vertices of that edge. In fact all the polynomial representations $f, f_n, f_s, f_{ss}, f_{ns}$ are uniquely determined through the three sides of the triangular element, and only f_{nn} is piecewise continuous, as it is the only derivative which depends on quantities specified at the third vertex of the triangle.

From the hydrodynamic view point $f = \psi$, f_n = tangential velocity component along an element edge and f_s is the normal velocity component on an element side. Since f, f_n and f_s are continuous through element sides then ψ and the velocity vector are everywhere continuous through the domain of solution, being C^1 and C^0 continuous, respectively.

The same arguments as above can be used for the heat transfer part of the problem to show that the temperature and heat flux vector are C^1 and C^0 continuous throughout Ω, respectively.

5. BOUNDARY CONDITIONS

Figure 2 shows the (8×8) regular finite element mesh and the boundary conditions used in this study.

The value of θ is set to 1 and zero at the nodes on the isothermal walls AD and BC, respectively. The first and second derivatives of θ with respect to the direction along these walls are also clearly zero and, following the arguments of the previous section, have been enforced at the boundary nodes to ensure that the variations of θ, θ_x and θ_{xx} are uniquely determined along the isothermal walls, and that at all points along these walls they retain

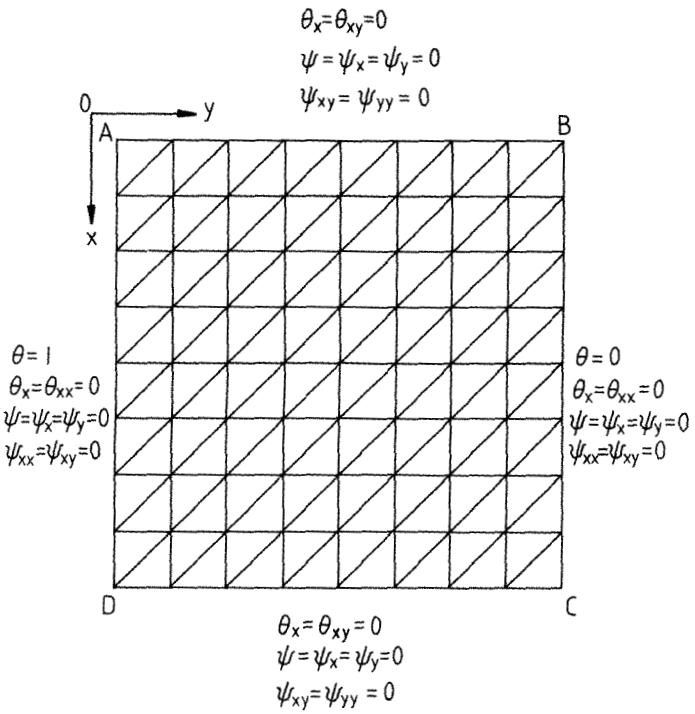

Figure 2. The (8×8) regular finite element mesh and boundary conditions

their enforced values. Similarly on the insulated walls AB and DC the nodal values of θ_x and θ_{xy} are set to zero, which ensures that $\theta_y = \theta_{xy} = 0$ is satisfied in pointwise fashion all along these walls.

Further, on all boundary nodes on the four walls conditions of impermeable and no-slip walls are rigidly satisfied by forcing both first derivatives of ψ to be zero at these nodes ($\partial\psi/\partial x = \partial\psi/\partial y = 0$). The value of ψ itself is arbitrarily defined as zero at all boundary nodes. Again here, it follows that the derivative of $\partial\psi/\partial n$ and the second derivative of ψ with respect to the direction along a wall are clearly zero ($\partial^2\psi/\partial x^2$ or $\partial^2\psi/\partial y^2 = 0$, and $\partial^2\psi/\partial n\partial s = \partial^2\psi/\partial x\partial y = 0$). Enforcing this at all boundary nodes ensures that $\psi = 0$, $u = v = 0$ is enforced pointwise along the entire boundary walls.

Since there are no singularities in the domain and on the boundaries of the problem, one can conclude that the four corner nodes A, B, C and D, which are intersection points between two walls, have boundary conditions equal to the union of the boundary conditions from the two adjacent walls. Therefore at all four corner nodes $\psi = \psi_x = \psi_y = \psi_{xx} = \psi_{xy} = \psi_{yy} = 0$, at nodes A and D $\theta = 1$, $\theta_x = \theta_{xx} = \theta_{xy} = 0$ and at nodes B and C $\theta = \theta_x = \theta_{xx} = \theta_{xy} = 0$.

It is important to note that, as a consequence of the above thermal boundary conditions, the gradient of the Nusselt number in the direction along the isothermal walls is zero at the two extremes of each isothermal wall. This is due to the fact that $\theta_{xy} = 0$ at the corners (i.e. $\partial Nu(x)/\partial x = 0$, since the local Nusselt number at any point on the isothermal walls $Nu(x) = \theta_y$). One would therefore expect a good numerical simulation to the double glazing problem to depict this feature accurately. Moreover, it can be used as a further validation check for the results from various codes.

6. NUMERICAL RESULTS

Three regular finite element grids (4×4), (5×5) and (8×8) were used to obtain results for four flow situations ($Ra = 10^3$, 10^4 and 10^5 with $Pr = 0{\cdot}71$); an additional solution on the

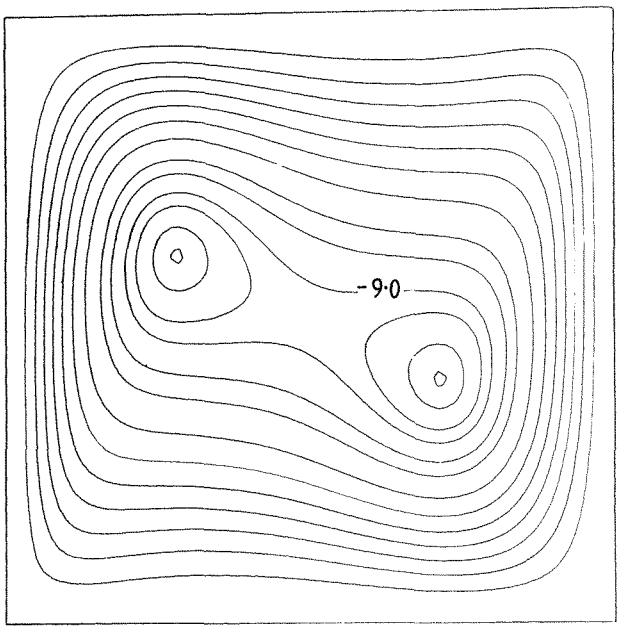

Figure 3. Stream function contours at $Ra = 10^5$ ($\Psi = 0(-1)-8, -8{\cdot}5, -9, -9{\cdot}25, -9{\cdot}5, -9{\cdot}6$)

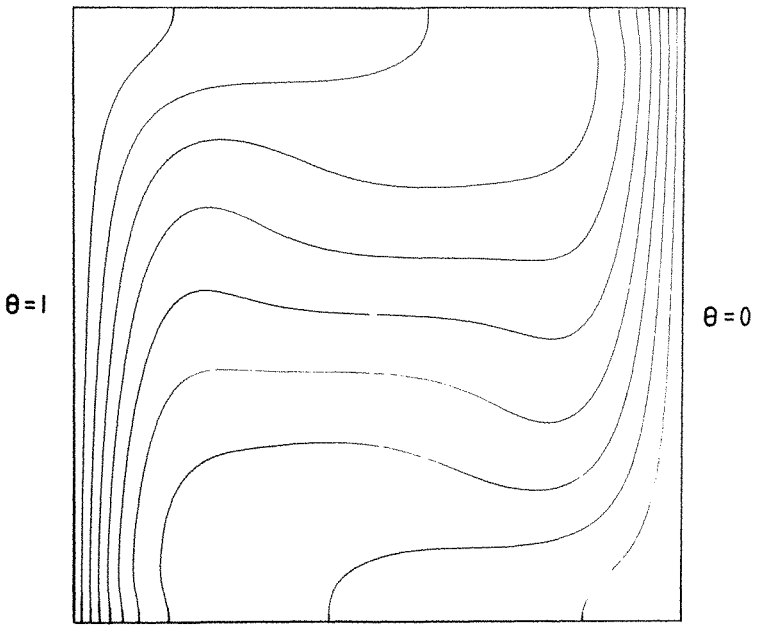

Figure 4. Temperature contours at $Ra = 10^5(\theta = 0{\cdot}0(0{\cdot}1)1{\cdot}0)$

(5×5) grid at $Ra = 10^6$ was also obtained. Owing to lack of space detailed results are only presented for solutions obtained from the (8×8) grid (Figures 3–5 and Tables I–III). However a summary of selected results for all flow situations, and all grids, is given in Table IV which includes number of iterations and the convergence tolerance ε. The results of all the tables were obtained from the true finite element interpolation on an (81×81) grid, thus all reported data (except $\overline{Nu} = \int_0^1 \theta_y|_y^{dx}$) are nodal values of this subgrid.

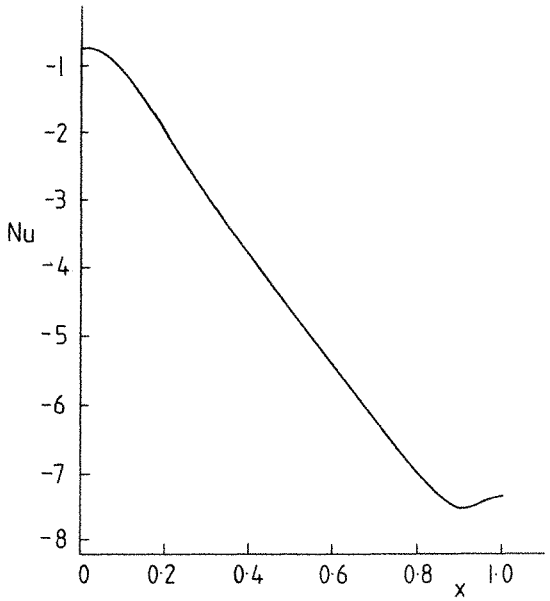

Figure 5. Nusselt number variation, along the hot wall $(y = 0{\cdot}0)$ at $Ra = 10^5$

Table I. $x = 0{\cdot}5$, horizontal mid-plane results

	$Pr = 0{\cdot}71$											
	$Ra = 10^3$				$Ra = 10^4$				$Ra = 10^5$			
y	ψ	v	u	θ	ψ	v	u	θ	ψ	v	u	θ
0·0	0·0	0·0	0·0	1·0	0·0	0·0	0·0	1·0	0·0	0·0	0·0	1·0
0·05	−0·05407	0·03048	−2·001	0·9434	−0·3956	0·4004	−14·1	0·8798	−2·051	0·675	−65·91	0·7716
0·1	−0·1857	0·09370	−3·139	0·8871	−1·261	1·054	−19·29	0·7656	−5·375	0·5252	−59·06	0·5938
0·15	−0·3572	0·1493	−3·633	0·8317	−2·232	1·215	−18·89	0·6672	−7·679	−2·735	−33·43	0·5001
0·2	−0·5413	0·1817	−3·666	0·7778	−3·107	0·9123	−15·84	0·5920	−8·822	−5·256	−13·79	0·4713
0·25	−0·7185	0·1892	−3·375	0·7261	−3·804	0·4094	−12·05	0·5414	−9·222	−6·133	−3·644	0·4725
0·3	−0·8754	0·1732	−2·874	0·6768	−4·318	−0·05103	−8·605	0·5119	−9·288	−5·735	0·3324	0·4813
0·35	−1·004	0·1408	−2·240	0·63	−4·675	−0·3341	−5·771	0·4978	−9·237	−4·677	1·355	0·4894
0·4	−1·098	0·09824	−1·527	0·5853	−4·905	−0·3803	−3·514	0·4938	−9·171	−3·256	1·224	0·4948
0·45	−1·156	0·05032	−0·7726	0·5422	−5·033	−0·2397	−1·659	0·4956	−9·122	−1·664	0·6554	0·4980
0·5	−1·175	0·0	0·0	0·5000	−5·074	0·0	0·0	0·5000	−9·107	0·0	0·0	0·5000

Table II. $y = 0{\cdot}5$, vertical mid-plane results

	$Pr = 0{\cdot}71$											
	$Ra = 10^3$				$Ra = 10^4$				$Ra = 10^5$			
x	ψ	v	u	θ	ψ	v	u	θ	ψ	v	u	θ
0·0	0·0	0·0	0·0	0·6341	0·0	0·0	0·0	0.7839	0·0	0·0	0·0	0·8116
0·05	−0·0512	1·901	−0·01161	0·6350	−0·2312	8·599	0·1461	0·7832	−0·5286	19·83	1·386	0·8099
0·1	−0·1771	3·021	−0·03964	0·6351	−0·8015	13·67	0·4408	0·7769	−1·846	31·46	4·38	0·801
0·15	−0·3434	3·549	−0·07391	0·6320	−1·552	15·91	0·6807	0·7615	−3·533	34·67	7·207	0·7824
0·2	−0·5247	3·639	−0·1053	0·6244	−2·357	16·01	0·8086	0·7365	−5·202	31·28	8·642	0·7561
0·25	−0·7020	3·409	−0·1269	0·6122	−3·128	14·63	0·8390	0·7037	−6·607	24·60	8·614	0·7246
0·3	−0·8618	2·951	−0·1324	0·5956	−3·805	12·34	0·7857	0·6659	−7·655	17·41	7·378	0·6893
0·35	−0·9945	2·334	−0·1204	0·5751	−4·353	9·507	0·6633	0·6253	−8·365	11·21	5·519	0·6491
0·4	−1·093	1·610	−0·09148	0·5517	−4·752	6·42	0·4833	0·5836	−8·801	6·507	3·553	0·6034
0·45	−1·154	0·8208	−0·04921	0·5264	−4·993	3·225	0·2553	0·5418	−9·034	2·955	1·718	0·553
0·5	−1·175	0·0	0·0	0·5000	−5·074	0·0	0·0	0·5000	−9·107	0·0	0·0	0·5000

Table III. Local Nusselt number distribution along hot wall at $y = 0{\cdot}0$

x	$Ra = 10^3$	$Ra = 10^4$	$Ra = 10^5$
0·0	−0·6912	−0·5847	−0·7273
0·05	−0·6935	−0·6034	−0·8187
0·1	−0·7026	−0·6658	−1·083
0·15	−0·7212	−0·7815	−1·502
0·2	−0·7516	−0·9503	−2·007
0·25	−0·7936	−1·157	−2·498
0·3	−0·8471	−1·391	−2·949
0·35	−0·9102	−1·642	−3·394
0·4	−0·9801	−1·900	−3·824
0·45	−1·055	−2·156	−4·223
0·5	−1·132	−2·408	−4·627
0·55	−1·207	−2·649	−5·032
0·6	−1·279	−2·874	−5·429
0·65	−1·345	−3·078	−5·847
0·7	−1·401	−3·252	−6·234
0·75	−1·447	−3·389	−6·636
0·8	−1·479	−3·480	−7·005
0·85	−1·497	−3·516	−7·302
0·9	−1·5057	−3·490	−7·531
0·95	−1·505	−3·422	−7·462
1·0	−1·503	−3·382	−7·361

Benchmark results for the double-glazing problem, produced for the Venice comparison study[9] by de Vahl Davis[8] are also listed in Table V. These have been modified to be consistent with the co-ordinate system presented here.

The sparse matrix solution routine[14] used in the current version of our code is an in-core solution routine. Solutions to the (4×4) and (5×5) grids were obtained on the CDC-7600 computer of UMRCC. This computer was, however, unable to satisfy the memory requirements of the (8×8) mesh; the solutions to this were obtained on a DEC VAX 11/750 computer which is a virtual memory machine. Single precision word lengths were used for all real variables in the two computers. However, it should be noted that the single precision word length on the CDC-7600 computer is twice that of the DEC VAX 11/750.

Solutions obtained from the (4×4) and (5×5) grids on the CDC-7600 computer reflected perfectly the symmetric nature of the flow. The solutions obtained from the (8×8) grid on the DEC VAX 11/750 machine, however, were to a slight degree asymmetric. The degree of asymmetry did not seem to increase with Ra, although it did increase with the order of the derivative of the variable in question. That is the temperature and stream function fields were virtually unaffected and thus symmetric. The velocities and the temperature first derivatives were slightly affected (the worst case being $\approx 0{\cdot}1$ per cent of the value). Finally the three second derivatives of the two main variables ψ and θ were the most affected (the worst case being ± 1 per cent of the value). As a further check on the validity of the DEC VAX 11/750 computer solutions, a solution to $Ra = 10^3$ on a (4×4) grid was obtained on this computer. This particular solution was compared to its equivalent obtained on the CDC-7600 computer. It was found that as far as the parameters of interest, in Tables IV and V, were concerned the two solutions were virtually identical, the asymmetries in the second derivatives on the VAX were comparable with those from the (8×8) grid above.

Table IV. Summary of selected results

		$Pr = 0{\cdot}71$			
	Mesh \ Ra	10^3	10^4	10^5	10^6
u_{max}	4×4	−3·712 at y = 0·175	−19·93 at y = 0·125	−67·11 at y = 0·075	—
at	5×5	−3·693 at y = 0·175	−19·87 at y = 0·1125	−70·79 at y = 0·075	−202·6 at y = 0·0625
$x = 0{\cdot}5$	8×8†	−3·698 at y = 0·175	−19·57 at y = 0·1125	−69·05 at y = 0·0625	—
v_{max}	4×4	3·659 at $x = 0{\cdot}1875$	16·25 at $x = 0{\cdot}175$	35·45 at $x = 0{\cdot}15$	—
at	5×5	3·647 at $x = 0{\cdot}1875$	16·17 at $x = 0{\cdot}175$	34·51 at $x = 0{\cdot}15$	64·91 at $x = 0{\cdot}1625$
y = 0·5	8×8†	3·651 at $x = 0{\cdot}1875$	16·18 at $x = 0{\cdot}175$	34·67 at $x = 0{\cdot}15$	—
	4×4	−1·114	−2·212	−4·497	—
$\overline{Nu}$	5×5	−1·116	−2·221	−4·489	−8·827
	8×8†	−1·117	−2·236	−4·467	—
Nu_{max}	4×4	−1·506 at $x = 1{\cdot}0$	−3·428 at $x = 0{\cdot}85$	−7·608 at $x = 1{\cdot}0$	—
at	5×5	−1·505 at $x = 0{\cdot}9375$	−3·463 at $x = 0{\cdot}85$	−7·593 at $x = 0{\cdot}9625$	−15·74 at $x = 1{\cdot}0$
y = 0·0	8×8†	−1·506 at $x = 0{\cdot}9125$	−3·516 at $x = 0{\cdot}85$	−7·536 at $x = 0{\cdot}9125$	—
Nu_{min}	4×4	−0·692 at $x = 0{\cdot}0$	−0·587 at $x = 0{\cdot}0$	−0·802 at $x = 0{\cdot}0$	—
at	5×5	−0·691 at $x = 0{\cdot}0$	−0·584 at $x = 0{\cdot}0$	−0·759 at $x = 0{\cdot}0$	−1·212 at $x = 0.0$
y = 0·0	8×8†	−0.691 at $x = 0.0$	−0·585 at $x = 0.0$	−0·727 at $x = 0{\cdot}0$	—
ψ_{max}	4×4	—	—	−9·52 at (0·4, 0·35)	—
at	5×5	—	—	−9·62 at (0·3875, 0·2875)	−18·37 at (0·4875, 0·15)
(x, y)	8×8†	—	—	−9·606 at (0·4, 0·2875)	—
	4×4	−1·174	−5·078	−9·207	—
$\psi(\frac{1}{2}, \frac{1}{2})$	5×5	−1·174	−5·0715	−9·045	−16·216
	8×8†	−1·175	−5·074	−9·107	—
Number	4×4	7	13	48	—
of	5×5	6	9	39	133*
iterations	8×8†	6	13	49	—
	4×4	0·001	0·001	0·001	—
ε (per cent)	5×5	0·01	0·01	0·01	0·01
	8×8†	0·005	0·001	0·001	—

* Denotes that intermediate steps of $Ra = 10^5$ and $Ra = 5 \times 10^5$ were used.
† Denotes that computations were performed on a DEC VAX 11/750 computer.

Table V. The benchmark solution[8]

Ra	10^3	10^4	10^5	10^6
u_{max} at $x=0{\cdot}5$	$-3{\cdot}697$ at $y=0{\cdot}178$	$-19{\cdot}617$ at $y=0{\cdot}119$	$-68{\cdot}59$ at $y=0{\cdot}066$	$-219{\cdot}36$ at $y=0{\cdot}0379$
v_{max} at $y=0{\cdot}5$	$3{\cdot}649$ at $x=0{\cdot}187$	$16{\cdot}178$ at $x=0{\cdot}177$	$34{\cdot}73$ at $x=0{\cdot}145$	$64{\cdot}63$ at $x=0{\cdot}15$
$\bar{Nu}$	$-1{\cdot}118$	$-2{\cdot}243$	$-4{\cdot}519$	$-8{\cdot}8$
Nu_{max} at $y=0{\cdot}0$	$-1{\cdot}505$ at $x=0{\cdot}908$	$-3{\cdot}528$ at $x=0{\cdot}857$	$-7{\cdot}717$ at $x=0{\cdot}919$	$-17{\cdot}925$ at $x=0{\cdot}9622$
Nu_{min} at $y=0{\cdot}0$	$-0{\cdot}692$ at $x=0{\cdot}0$	$-0{\cdot}586$ at $x=0{\cdot}0$	$-0{\cdot}729$ at $x=0{\cdot}0$	$-0{\cdot}989$ at $x=0{\cdot}0$
ψ_{max}	—	—	$-9{\cdot}612$ at $x=0{\cdot}399$ $y=0{\cdot}285$	$-16{\cdot}75$ at $x=0{\cdot}453$ $y=0{\cdot}151$
$\psi(\frac{1}{2},\frac{1}{2})$	$-1{\cdot}174$	$-5{\cdot}071$	$-9{\cdot}111$	$-16{\cdot}32$

As noted previously a decoupled (segregated) solution scheme was used. Experience showed that a single Newton–Raphson iteration per equation step was appropriate for all situations with the latest temperature value only damped for cases of high Ra. Solutions above $Ra = 10^3$, for all grids, required increasing degrees of damping. For $Ra = 10^4$ on grids (4×4) and (8×8) the latest temperature update was damped by 40 per cent (i.e. 40 per cent old − 60 per cent new). On the (5×5) mesh for the same Ra the latest temperature and stream function vectors were damped by 30 per cent. At $Ra = 10^5$ 80 per cent damping was used on the temperature for all grids. The $Ra = 10^6$ solution of the (5×5) grid was only possible with very heavy damping of the temperature—95 per cent. It should be noted that damping the temperature field was required solely for stability purposes and not for accelerating convergence. In fact increasing Ra (and damping) decreased the rate of convergence. This can be seen in pictorial fashion in Figure 6 where convergence data from the (8×8) grid is presented. As is indicated on this Figure and Table IV, the convergence tolerance ε was forced to assume smaller values when damping was being used. This was done to ensure that the temperature solution had also converged. Note that when heavy damping is employed on one parameter (temperature, here) the other (stream function) might approach the solution at a much slower rate and give the false impression of convergence. Thus, in order to avoid this, the tolerance criterion was made more stringent. Further, when this criterion was satisfied the pre and post-damped temperature fields were checked to ensure that they were indeed identical.

The relatively poor convergence characteristics at high Ra for the present method seem to be due to the segregated (decoupled) method of solution (cf. Reference 15). This aspect is discussed further in the next section.

The need to damp temperature in the above is strongly signalling the fact that the problem is more sensitive to temperature changes than hydrodynamic changes. A small change in the temperature field resulted in a large change in the velocity field, whereas the opposite was not true for changes in the hydrodynamics. It is felt that this is a reflection of the actual physical response characteristics of the double glazing flow problem. Hence in order to represent this characteristic correctly, all numerical simulations to this problem should use

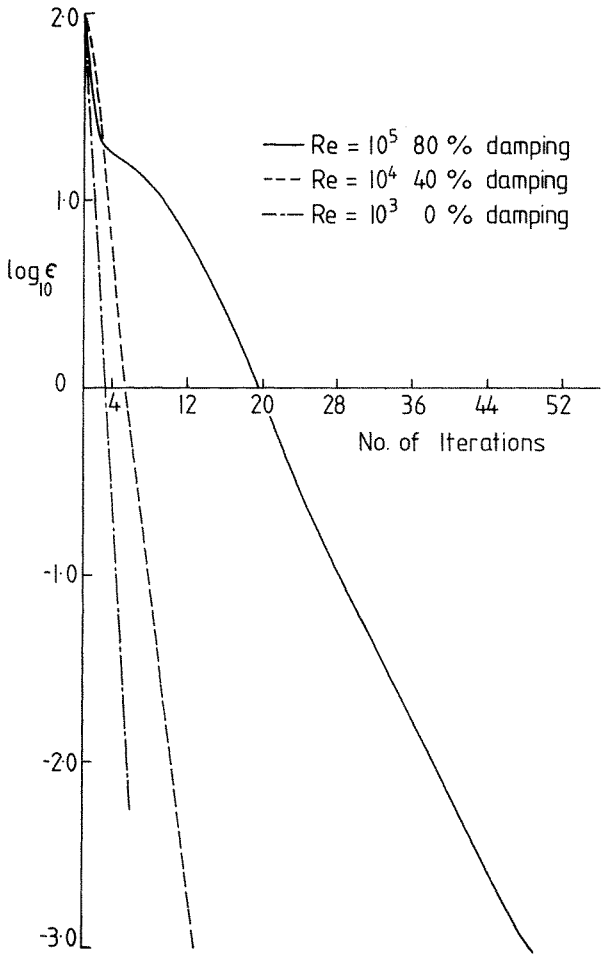

Figure 6. Convergence criterion; $\log_{10} \varepsilon$ vs number of iterations

higher order temperature polynomial representations than velocities. This point may be particularly relevant in the primitive variable solution to the problem, where it is standard practice to use equal order polynomial representations for velocities and temperature. We feel that higher order representations for temperature (in comparison with representations for velocity) will improve the convergence and accuracy of the above primitive variable simulations.

Results at $Ra = 10^6$, for the (8×8) grid, were not obtained owing to lack of time. Computations on the (8×8) grid were rather costly in time in that they required half an hour of CPU time per iteration on the slower DEC VAX 11/750 machine. An iteration consists of a single solution of the Newton–Raphson step for stream function, plus a single solution of the temperature equation. An equivalent iteration at any Ra on the (4×4) grid with the CDC-7600 required 13 seconds of CPU time.

The solution to $Ra = 10^6$ obtained from the (5×5) mesh has been included in Table IV merely to demonstrate that such a high Ra solution is feasible by the present method. It is not claimed, however, that this solution is accurate, and it should not be considered for comparison purposes.

7. DISCUSSION OF RESULTS AND METHOD

The results from our finest mesh (8×8) compare favourably with those in Table V. This is especially gratifying to see since the benchmark results were obtained by extrapolating to zero mesh size, from the solution of successively finer grids.[8]

A comparison of the total free degrees of freedom shows that the (8×8) grid of the present study has 731 whereas the finest grid, (81×81), of the study of de Vahl Davis[8] has 18871 free degrees of freedom. This is a further indicator of the resolution capabilities of the present method.

A careful comparison of the present and benchmark solutions, Tables IV and V, reveals that there is better agreement between hydrodynamic than thermodynamic quantities. For example, at $Ra = 10^5$ the value of the maximum Nusselt number in Table IV is 2·3 per cent lower than that of the benchmark value, whereas the worst hydrodynamic discrepancy at the same Ra is 0·7 per cent (u_{max}).

The question posed about the expected variation of $Nu(x)$ near the extremes of the isothermal walls in the final paragraph of Section 5 can now be studied. Figure 5 shows the Nusselt number variation along the hot wall at $Ra = 10^5$. It is quite clear from this figure that at the two extremes of this curve (corners A and D, see Figure 2) $\partial Nu(x)/\partial x = 0$.

A similar plot by de Vahl Davis[8] (Figure 2 of his report) at $Ra = 10^6$ showed values of $\partial Nu(x)/\partial x \neq 0$ at the corner, even with the finest mesh used; (81×81). De Vahl Davis produced this Figure to demonstrate that in his study the variation of Nu_{max} with grid refinement at $Ra = 10^6$ was not monotonic. His Figure shows further that there is a monotonic increase of the value of the Nusselt number in the corner, which suggests a higher value of local Nu there.

Figure 7 shows an exaggerated version of Figure 5 in the corner region, on this are also superimposed the detailed results of Winters[15] and Upson *et al.*[15], which were kindly provided by Winters and P. M. Gresho (Private Communications).

The results of Winters were calculated at element level, and since he used quadratic elements, the temperature gradients are discontinuous across element boundaries. Consequently the values given at common nodes between two elements were the arithmetic means from each side. Upson *et al.*, however, used the consistent flux method[15] to obtain their heat flux levels.

The solutions produced by the above authors were considered to be among the most accurate in the comparison exercise of de Vahl Davis and Jones.[16] It is clear from Figure 7 that the condition of $\partial Nu(x)/\partial x = 0$ at $x = 1{\cdot}0$ is not met by the curves of Winters and Upson *et al.* whereas the curve of the present solution is compelled to satisfy this condition exactly. Further, the curve of the present solution produces a higher value of local Nusselt number at $x = 1{\cdot}0$ whereas the value of Nu_{max} is lower by 2·5 per cent from that of the other two contributions. Moreover, the results in Table IV suggest that the value of Nu_{max} obtained from the present solution has converged, with grid refinement, to a tolerance well below a 2·5 per cent truncation error.

Both Winters and Upson *et al.* used the Galerkin finite element method with mesh refinement into the corner. Consequently, the imposition of the insulated condition on the top and bottom walls was only of the weak form. Similarly in the benchmark solution[8] no equations are solved for the corner nodes themselves. Thus, although these three solutions agree to within 0·3 per cent for Nu_{max} it is not surprising that they fail to satisfy the correct condition $\partial Nu(x)/\partial x = 0$ at the corner. It is noticeable that the results of Winters[15] and Upson *et al.*[15] tend towards this condition at the lower Ra values, where the present results

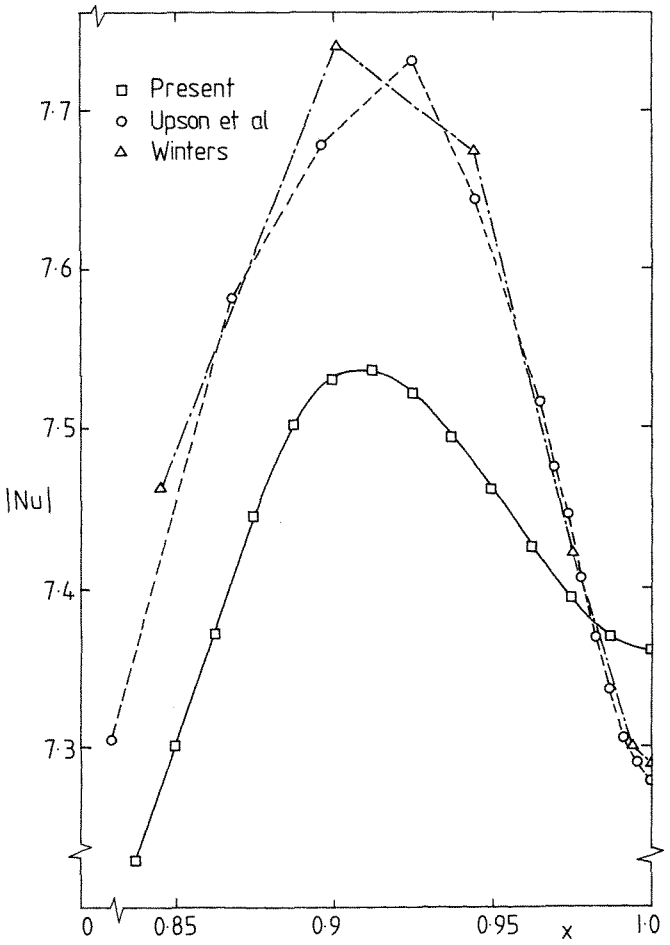

Figure 7. A comparison of local Nusselt number distributions near the bottom hot wall corner at $Ra = 10^5$

for Nu_{max} are in better agreement. It is our belief that the present results for Nu_{max} are therefore more accurate than the benchmark solution and that the effect of imposing the condition $\partial Nu(x)/\partial x = 0$ at the corners is to decrease the value of Nu_{max} as well as increasing the value of Nu in the corner. It is unfortunate that, with the present high-storage solution routine, time was not available to obtain results at $Ra = 10^6$ on a finer mesh than (5×5), since the uncertainties in the benchmark Nusselt number values must then be even greater than at $Ra = 10^5$. Note that these differences are not noticeable in the region of Nu_{min}.

In addition to its resolution capabilities, a further merit of the present method is that all parameters of interest (i.e. ψ, $u = \psi_y$, $v = -\psi_x$, $\omega = \psi_{xx} + \psi_{yy}$, θ and $Nu = \theta_y|_{y=0,1}$) except pressure are automatically available from the solution. Pressure solutions can be recovered in a post processor code, details of this are given by Haroutunian.[11]

The present method also automatically provides for a higher order polynomial representation for temperature than for velocities. In the previous section this was suggested as being desirable for better accuracy and convergence.

In spite of its attractive features, the method suffers from three inherent disadvantages. First, setting-up times are somewhat expensive compared to other more conventional finite

element methods. However, for a given grid, time can be saved by grouping identical elements (as in regular grid situations) and also by using a preprocessor code for obtaining element contribution matrices and storing them on magnetic tape for multiple further usage. Secondly, since the number of degrees of freedom per node in this method of solution is high compared to other methods, the bandwidth of the associated system of discretized equations is large. Further, the present decoupled (segregated) solution scheme gives rise to slow convergence and necessitates heavy damping for retaining stability at high Ra. A coupled (direct) solution scheme as opposed to a segregated one would certainly speed up convergence and increase stability (less need for damping). However, this will further aggravate the problem relating to storage requirements in that it will increase the DOF per node, and hence the bandwidth, by a factor of two. A more viable alternative is to adopt the technique used by Gartling.[15] In his solution to the double glazing problem using a segregated type solution to the primitive variables formulation, he had to change from a steady state type approach to a time-dependent scheme (still retaining his segregated scheme) in order to obtain solution for the $Ra > 10^4$. Such a scheme also seems attractive here and should similarly improve the stability and radius of convergence characteristics of our method. Note that the problem seems less acute with the present formulation, since Gartling only reports steady state type solutions up to $Ra = 10^4$, whereas results were obtained up to $Ra = 10^6$ here. The problem of large bandwidths for finer grids would however still remain. This problem can be tackled by using disc based (out of core) solution routines.

The final disadvantage of the method is that the stream function formulation strategy will not extend in a straightforward fashion to three dimensions (c.f. Reference 10). Indeed, it seems unlikely that such an extension could be a practicable proposition.

8. CONCLUSIONS

The stream function solution to the two-dimensional double-glazing problem, in conjunction with the 18 DOF truncated quintic triangular finite element, shows considerable promise by producing accurate results on relatively coarse meshes. In contrast to most conventional solution methods, the imposition of the insulation boundary condition can be achieved in pointwise fashion all along the insulated walls. As a direct consequence of this, it is argued that the Nu_{max} values produced at high Ra by this simulation are more accurate than the benchmark values.[8] In addition, the relative orders of representation of velocity and temperature have a favourable effect on the accuracy of the temperature solution.

REFERENCES

1. R. L. Sani, P. M. Gresho, R. L. Lee and D. F. Griffiths, 'The cause and cure (?) of the Spurious Pressure Generated by certain FEM solutions of the incompressible Navier–Stokes equations', *Int. J. Num. Meth. Fluids*, **1,** 17–43 (1981) and **1,** 171–204 (1981).
2. C. P. Jackson and K. A. Cliffe, 'Mixed interpolation in primitive variable finite element formulations for incompressible flow', *Int. J. Num. Meth. Engng.*, **17,** 1659–1688 (1981).
3. B. Tabarrok and R. C. Lin, 'Finite element analysis of free convection flows', *Int. J. Heat Mass Transfer*, **20,** 945–952 (1977).
4. S. L. Smith and C. A. Brebbia, 'Finite element solution of Navier–Stokes equations for transient two-dimensional incompressible flow', *J. Comp. Phys.*, **17,** 235–245 (1975).
5. W. N. R. Stevens, 'Finite element, stream function–vorticity solution of steady laminar natural convections', *Int. J. Num. Meth. Fluids*, **2,** 349–366 (1982).
6. S. Y. Tuann and M. D. Olson, 'Studies of rectangular cavity flow with Reynolds number by a finite element method', *Structural Research Series, Report No. 19*, Dept. Civil Eng. U.B.C., Vancouver, Canada, 1977.
7. S. Y. Tuann and M. D. Olson, 'Numerical studies of the flow a circular cylinder by a finite element method', *Structural Research Series, Report No. 16*, Dept. Civil Eng., U.B.C., Vancouver, Canada, 1976.

8. G. de Vahl Davis, 'Natural convection of air in a square cavity: a bench mark numerical solution', *Int. J. Num. Meth. Fluids*, **3,** 249–264 (1983).
9. G. de Vahl Davis and I. P. Jones, 'Natural convection in a square cavity: a comparison exercise', in R. W. Lewis, K. Morgan and B. A. Schrefler (eds) *Numerical Methods in Thermal Problems*, Vol. II. Pineridge Press, Swansea, U.K., 552–572 (1981).
10. G. D. Mallinson and G. de Vahl Davis, 'Three-dimensional natural convection in a box: a numerical study', *J. Fluid Mech.* **83,** 1–31 (1977).
11. V. Haroutunian, 'A stream function finite element solution for natural convection', *M.Sc. Dissertation*, UMIST, Manchester, January 1981.
12. G. R. Cowper, E. Kosko, G. M. Lindburg and M. D. Olson, 'Static and dynamic applications of a high precision triangular plate bending element', *AIAA Journal*, **17,** 1957–1965 (1969).
13. G. R. Cowper *et al.*, 'A high precision triangular plate bending element', *Aeronautical Rept. LR-514*, National Research Council of Canada, December 1968.
14. S. K. Gupta and K. K. Tanji, 'Computer program for solution of large, sparse unsymmetric systems of linear equations', *Int. J. Num. Meth. Engng*, **11,** 1251–1259 (1977).
15. I. P. Jones and C. P. Thompson (eds.), *Numerical solution for a Comparison Problem on Natural Convection in an Enclosed Cavity*, AERE-R9955, HMSO, 1981.
16. G. de Vahl Davis and I. P. Jones, 'Natural convection in a square cavity: a comparison exercise', *Int. J. Num. Meth. Fluids*, **3,** 227–248 (1983).